ICAS-82-2.5.3

A NEW TESTING METHOD OF IMPULSIVE BEHAVIOUR FOR AEROSPACE MATERIALS

K. Kawata, S. Hashimoto and N. Takeda

Institute of Interdisciplinary Research
Faculty of Engineering, University of Tokyo
Komaba, Meguro-ku, Tokyo, Japan

Abstract

Facts on high-velocity ductility and brittleness of metallic materials are shown to stress the crystal lattice systems effect. Constitutive equations for BCC and FCC metals are introduced modelling mild steel and high-strength Al alloys, respectively, on the basis of micromechanics of dislocations. Then, these constitutive equations are used to analyze the elasto-plastic wave propagation in BCC and FCC metals, by the finite element method (FEM). Clear difference between two metals such as existence and non-existence of a sharp stress peak at the wave front is found.

Through comparison of various high-velocity tension testing methods using FEM and the specimen constitutive equations, a new testing method--one bar method--of block-to-bar type is devised for its accuracy and simplicity. Formulae for dynamic stress and strain are derived based upon the one-dimensional stress wave propagation theory, and a new testing machine for material characterization in high-velocity tension is constructed. The major feature of this new machine is that dynamic tensile stress-strain diagrams are obtained up to the breaking strain immediately after the test.

Typical experimental data obtained on a mild steel and an Al alloy show critical differences in material behaviour in high-velocity tension, as expected in the theoretical analysis. On the other hand, experimental data on typical composite materials reveal that there are tendencies of high-velocity ductility for GFRP and of high-velocity brittleness or insensitivity for CFRP. Then, circumferentially V-notched specimens of GFRP are introduced for the measure of material characterization based upon fracture mechanics, which cannot be obtained with straight specimens.

1. Introduction

In spite of recent increasing demands for impact-resistant structures for aerospace use, mechanical behaviour of aerospace materials under impulsive loading conditions is not well known. This is mainly due to the fact that reliable impact testing methods have not sufficiently been developed so far. There exist several impact testing methods, among which Charpy or Izod impact methods are most commonly used. Although impact tests of Charpy or Izod type are easy to conduct, they contain substantial disadvantages. They only give absorbed energy (and applied force in instrumented tests). Moreover, since they are essentially impact bending tests of short beams, data from them are difficult to interpret due to the stress complexity which involves shear, tension and compression and which is different from that in real structures. Comparison of these data can be made only if one standard test with the same dimensions of specimens and apparatuses. Thus, these data are not applicable directly in designing real structures, unlike quasi-static test data. Hence, demands for impact testing methods which isolate a single stress or strain state have been increasing, especially in designing impact-resistant structures.

Above all, material characterization in impulsive or high-velocity tension is most fundamental, but there has been little progress in its measuring techniques. For the establishment of a precise design for impact-resistant structures, exact material characterization in high-velocity tension --dynamic tensile stress-strain relation determination up to breaking strain--has been an urgent necessity.

To obtain a practical high-velocity tension testing system as precise and as simple as possible in character, systematic investigations of impact responses of various possible testing systems are carried out. That is, finite element numerical analysis for model responses of these testing systems is performed with specimens of BCC and FCC metallic materials which are well represented by their own constitutive equations of the microscopic origin. Through these systematic investigations, one bar method of block-to bar type is adopted as a precise and simple system. Then the authors construct a new high-velocity tensile stress-strain measuring system of one bar method, and derive formulae for dynamic stress and strain using the one-dimensional stress wave propagation theory. With this new testing system, high-velocity tensile stress-strain diagrams up to breaking strain are obtained for several aerospace materials which include metallic materials (BCC and FCC metals) and composite materials (GFRP and CFRP), and new concepts of high-velocity brittleness and ductility are introduced for both metallic and composite materials.

2. Micromechanics of High-Velocity Deformation of Metallic Materials

2.1 High-Velocity Ductility and Brittleness

The results of high-velocity tension tests of pure metals and alloys in annealed state covering the tensile velocity range from 10^{-5} m/s to 200 m/s (equivalent strain rate: 2×10^{-4} /s to 4×10^{3} /s) by Kawata et al.[1] indicate the existence of the crystal lattice systems effect on increasing or decreasing of tensile breaking strain ε_b with increasing tensile velocity V_1, as shown in Fig. 1. Let β define the ratio of the maximum variation in ε_b to the static breaking strain ε_{bs} [2,3]. Then terms of high-velocity brittleness and high-velocity ductility are defined as to possess negative and positive values of β, respectively. The summary of β values is given in Table 1[2,3].

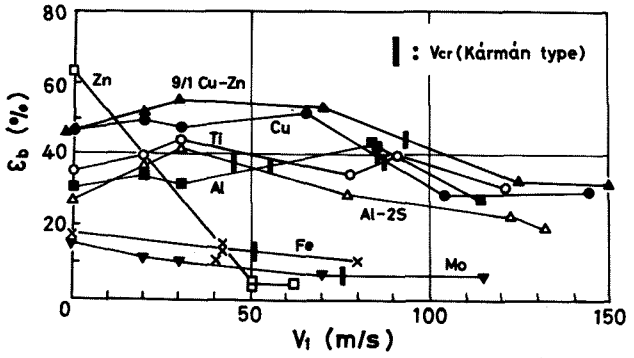

Figure 1. Breaking Strain ε_b vs. Tensile Velocity V_1 Relation in High-Velocity Tension of Annealed Pure Metals and Alloys[1]. V_{cr} is the critical velocity above which $\varepsilon_b=0$, according to the Kármán theory using a static stress-strain curve.

Table 1. Crystal Lattice Systems Effect on High-Velocity Breaking Strain[2,3].

Crystal lattice system	Material	Ratio of max. variation in ε_b to static breaking strain ε_{bs}, β (%)*
FCC	9/1 Cu-Zn	+20.0
	Cu	+11.3
	Al	+41.9
	Al-2S	+53.2
BCC	Fe	-40.1
	Mo	-56.6
HCP	Ti	+25.9
	Zn	-93.2

* $\beta<0$: High-Velocity Brittleness
$\beta>0$: High-Velocity Ductility

High-velocity brittleness appears for BCC metals, high-velocity ductility for FCC metals, and both high-velocity brittleness and ductility for HCP metals. The facts that Zn shows high-velocity brittleness and that Ti shows high-velocity ductility seem closely related to the axial ratio c/a of their HCP lattice systems. In ordinary temperatures now considered, the axial ratio is 1.856 for Zn, while 1.587 very close to the value of FCC metals for Ti. The above facts verify the necessity of micromechanics connected with crystal lattice systems in understanding the individuality of metallic materials in high-velocity deformation.

2.2 Constitutive Equations for BCC and FCC metals and Their Application to High-Velocity Deformation

Constitutive equations characteristic of the respective crystal lattice systems should be derived from the standpoint of micromechanics or dislocation theories. To derive constitutive equations, it is necessary to obtain the plastic strain rate $\dot{\varepsilon}_p$ which is the function of rate controlling deformation processes.

In BCC metals such as mild steel, the resistance to determine the dislocation velocity is based upon intrinsic resistance, that is, frictional force between crystal lattices and a dislocation. Plastic strain rate $\dot{\varepsilon}_p$ is given from the product of the Burgers vector, the number of movile dislocations and the dislocation velocity as an exponential function of shear stress. For BCC metal modelling mild steel, a constitutive equation deduced from the Johnston-Gilman type[4,5] plastic strain rate[6] is,

$$\dot{\varepsilon}-\frac{\dot{\sigma}}{E}=\frac{4}{3}b\left[N_0+\frac{3}{4}M\left(\varepsilon-\frac{\sigma}{E}\right)\right]v^*\exp\left(-\frac{2\left[D+\frac{3}{4}H\left(\varepsilon-\frac{\sigma}{E}\right)\right]}{\sigma}\right) \qquad (1)$$

for tensile stress σ and strain ε, where a dot($\dot{}$) denotes a time derivative. For a typical mild steel, constants in Eq. (1) are given as

$b=2.5\times10^{-7}$ mm, $v^*=3.2\times10^{6}$ mm/s, $N_0=3.75\times10^{4}$ /mm^2, $M=10^{9}$ /mm^2, $D=200$ kg/mm^2, $H=10666$ kg/mm^2, and $E=2.15\times10^{4}$ kg/mm^2.

High-strength Al alloy, a typical aerospace material, belongs to the FCC crystal lattice system. For Al and Al alloys in the strain rate range from 10^{-3} to 10^{3} /s, a constitutive equation derived from thermally activated motion of dislocations, based upon the experimental facts and their analyses[7-11], should be used. In FCC metals, intrinsic resistance is small for $\dot{\varepsilon}<10^{3}$ /s, and extrinsic resistance such as cutting of forest dislocations seems predominant, and this is considered thermally activated. When the consideration by Seeger[8] for Al is directly formulized, the form in Eq. (2) is obtained.

$$\dot{\varepsilon}-\frac{\dot{\sigma}}{E}=C\exp\left[-\frac{U_0}{kT}\left(1-\frac{\sigma}{\sigma_0}\right)\right] \qquad (2)$$

where E is Young's modulus, C frequency constant, U_0 activation energy, k Boltzmann's constant, T absolute temperature, and σ_0 constant related to activation volume. It is known that calculations based upon Eq. (2) give elastic, perfectly plastic behaviour[2]. So, for high-strength Al alloys showing strain hardening, terms corresponding to strain hardening and athermal stress should be introduced. The constitutive equation derived based upon the above-mentioned considerations is expressed by Eq. (3)[2],

$$\dot{\varepsilon}-\frac{\dot{\sigma}}{E}=C\exp\left[-\frac{U_0}{kT}\left(1-\frac{\sigma-\sigma_g}{\sigma_0\left(1+H\left(\varepsilon-\frac{\sigma}{E}\right)\right)}\right)\right] \qquad (3)$$

where the constants are $E=7190$ kg/mm^2, $C=4.5\times10^{12}$ /s, $U_0=30.3\times10^{-18}$ kgmm, and $\sigma_0=19.42$ kg/mm^2; and k is Boltzmann's constant, and T=300 K.
The values of H and σ_g depend on the kind of an Al alloy considered. In FCC metals for $\dot{\varepsilon}>10^{3}$ /s, intrinsic resistance seems to become predominant. So, to predict the material behaviour in this very high strain rate region, another approach will be needed.

The behaviours of elasto-plastic wave propagation in mild steel and high-strength Al alloys, respectively, are derived from Eqs. (1) and (3). The calculation is performed by combining[12, 13] the finite element method and the Newmark β method [2]. As typical examples, the behaviours of elasto-plastic waves in high-velocity tension of thin bars of finite length are shown. Figures 2 and 3

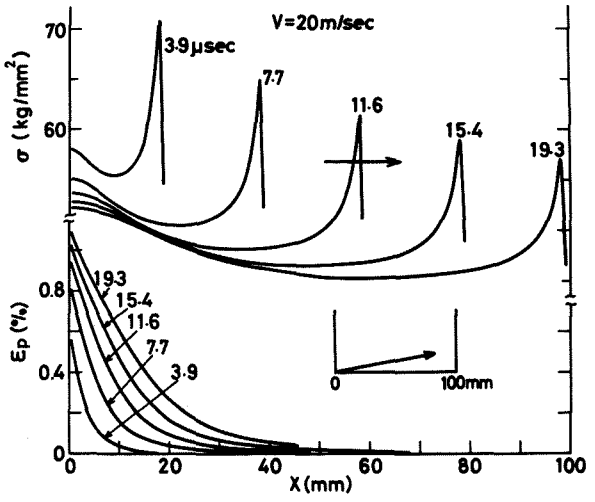

Figure 2. σ and ε_p distributions in high-velocity tension of a bar of a mild steel of finite length (V=20 m/s) before reflection[2].

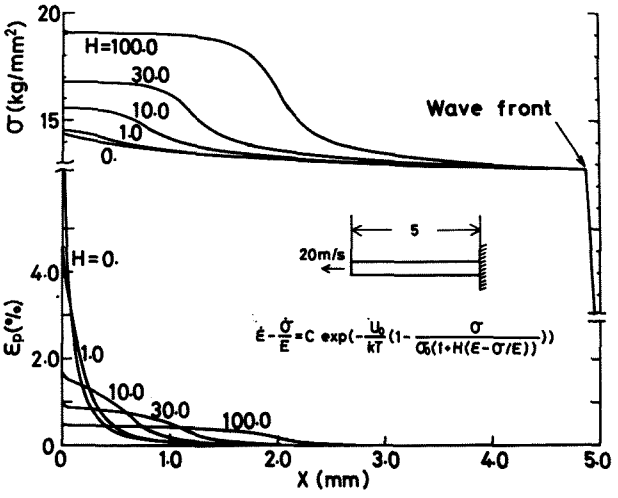

Figure 3. σ and ε_p distributions in high-velocity tension of a bar of finite length of an Al alloy governed by Eq. (3) before reflection (σ_g=0)[2].

correspond to mild steel and high-strength Al alloy, respectively. As shown clearly in these figures, a sharp stress peak appears at the stress wave front in the former case, and in contrast a sharp stress peak does not exist at the stress wave front in the latter case. This is one remarkable difference found between these crystal lattice systems. On the other hand, the fact that a plateau of plastic strain distribution is formed successively by the progress of strain hardening is common to both constitutive equations. These facts correspond well to the accumulated experimental data. As mentioned above, the individuality of metallic materials in high-velocity deformation and fracture is considered to be grasped and understood for the first time by introducing micromechanical considerations.

3. A New Testing Method of Material Behaviour in High-Velocity Tension

3.1 Comparison of Various High-Velocity Tension Testing Method

Systematic examination of the impact response of various high-velocity tension testing methods is carried out using the finite element method combined with the Newmark β method[14]. In this analysis, materials obeying to the constitutive equations, Eqs. (1) and (3), are used as test specimens.

Analyzed models for the testing methods are as follows:

(1) Block-to-block type
One end is pulled and the other end is fixed. The stress of the specimen cannot be obtained experimentally even if a strain gage is cemented on the specimen, because the output cannot determine stress for an undermined stress-strain relation.

(2) Block-to-block type with a short load cell
A load cell (steel bar with gages at the center) is added to the fixed end of case 1 mentioned above, to try to obtain the dynamic stress of the specimen. The cross-sectional area of the load cell is four times larger than that of the specimen. Results obtained from the relative displacement and average stress of both ends of the specimen is named case 2, and the result obtained from the output of the load cell is named case 2'.

(3) Block-to-bar type
To measure the stress and displacement, an output bar is added to the fixed end of the specimen of case 1.

(4) Bar-to-bar type
That is, the split Hopkinson bar type method for tension in which the given velocity is half the other cases, so that the induced strain in the specimen becomes equal to that in the other tests when the impedance of the specimen becomes zero compared with the input/output bars.

Figures 4 and 5 show the differences in the results from all cases of testing considered. Except case 2', stress-strain relations are almost equal for FCC material, but for BCC material differences are seen. The effect of the input/output bar appears to decrease the strain rate. For case 2', the effect of vibration of the load cell appears in both materials examined. It is concluded that case 2' is not successful for impact testing and that the response characteristics of each testing method are influenced by the individuality of specimen materials. Cases 3 and 4 give good responses in high-velocity tension. Since case 3, block-to-bar type, is preferable in its simplicity, the authors adopt this testing method in the following.

3.2 One Bar Method for Material Characterization in High-Velocity Tension

3.2.1 Fundamental[14]. To realize the block-to-bar type testing machine, analytical procedure of this method is established. Since this method uses only one bar, the authors call it "one bar method" hereafter. The testing machine consists of a hammer, an impact block, a specimen and an output bar (Fig. 6). When the impact block is impacted by the hammer, the specimen is deformed and the strain $\varepsilon_g(t)$ of the output bar is measured at a distance

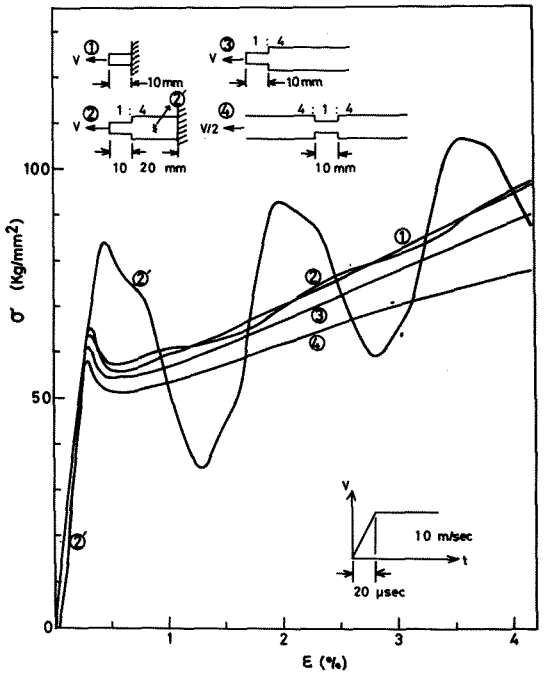

Figure 4. The differences in stress-strain relations obtained by various testing methods for high-velocity tension of BCC metal modelling a mild steel.

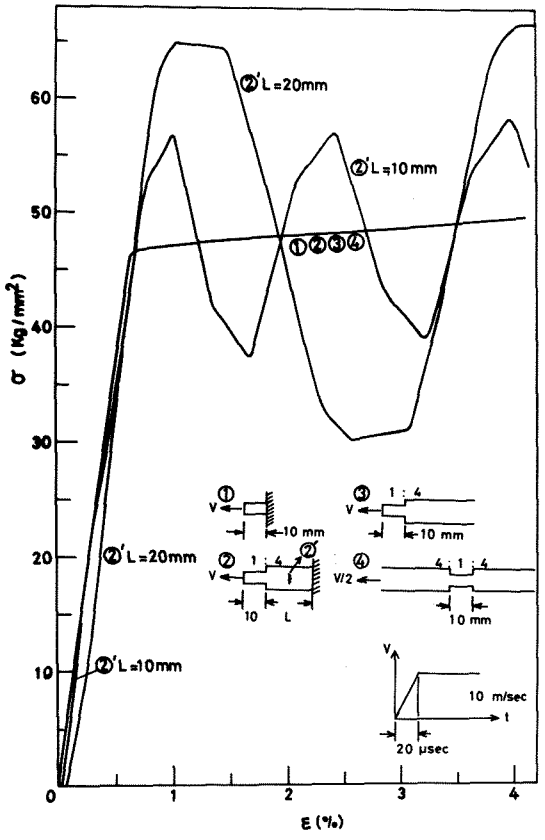

Figure 5. The differences in stress-strain relations obtained by various testing methods for high-velocity tension of FCC metal modelling 2014-T6 Al alloy (σ_g= 33 kg/mm^2, H=6.86)

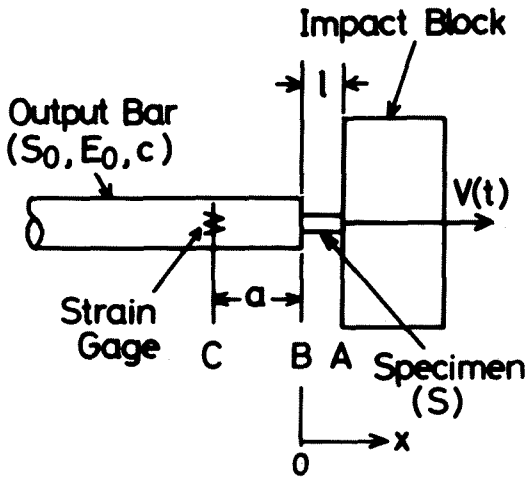

Figure 6. Analysis of one bar method of block-to-bar type.

of a from the impact end. The stress and strain of the specimen is calculated by the one-dimensional stress wave theory as follows,

$$\varepsilon(t) = \frac{1}{l}\int_0^t [V(\tau) - c\varepsilon_g(\tau+\frac{a}{c})]d\tau$$
$$\sigma(t) = (\frac{S_0}{S})E_0\varepsilon_g(t+\frac{a}{c}) \qquad (4)$$

where l and S are the length and the cross-sectional area of the specimen, and S_0, E_0 and c are the cross-sectional area, Young's modulus and the elastic wave velocity of the output bar. V(t) is the velocity of the impact block and is measured by an electro-optical extensometer. The derivation of Eq. (4) is given in the appendix.

3.2.2 Construction of Testing Machines. According to one bar method, two kinds of high-velocity tensile testing machines are costructed as shown in Figs. 7 and 8[3,14]. Testing machine A is a rotating disc-type testing machine shown in Fig. 7. At first the impact block is set vertical. When the desired speed of the disc is attained, a hook is released by a magnet and the impcat block is rotated by 90° by a coil spring. Thus the specimen is given high-velocity tension up to rupture. The maximum peripheral speed of the disc is about 100 m/s. Testing machine B is a pendulum-type testing machine, shown in Fig. 8. The hammer speed at the impacting point is 3.5 m/s.

In actual calculations, a calculating system for dynamic stress-strain diagrams shown in Fig. 9 is utilized. First the transient output-bar strain $\varepsilon_g(t)$ is recorded in a digital transient wave memory. Then combining it with an impact-block velocity V(t), a digital computer calculates dynamic stress σ(t) and strain ε(t) using Eq. (4), and also absorbed energy per unit volume $e(t)$, immediately after tests. The major feature of this testing machine is that dynamic tensile stress-strain diagrams are obtained up to the breaking strain immediately after tests.

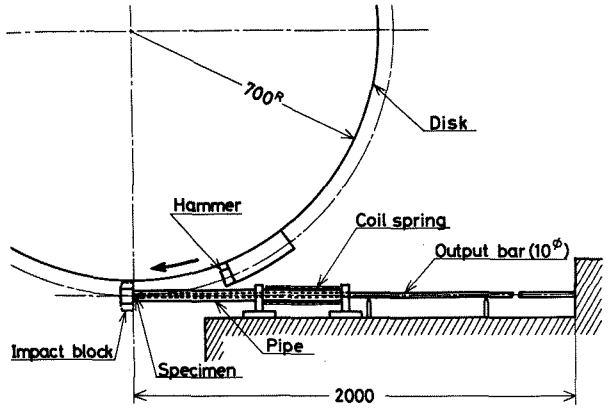

Figure 7. Testing machine A of a rotating-disc type.

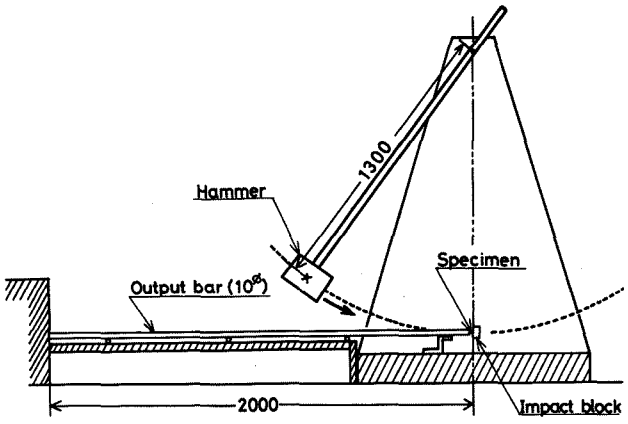

Figure 8. Testing machine B of a pendulum type.

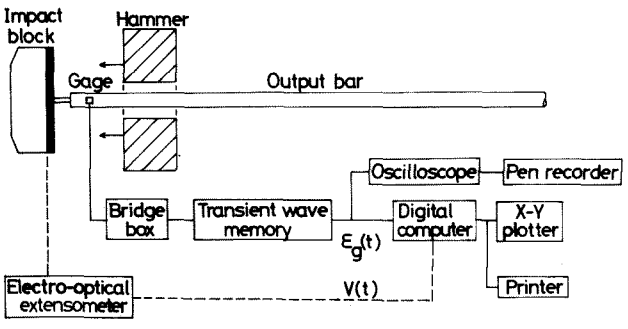

Figure 9. A calculating system for dynamic stress-strain diagrams.

4. Characterization of Aerospace Materials in High-Velocity Tension

4.1 Metallic Materials

Typical experimental results obtained by machine A are shown in Figs. 10 and 11 for metallic materials. Specimen dimensions used are shown in Fig. 12. A remarkably increasing rise in the upper yield point with increasing strain rate is clearly recorded for a mild steel S45C (0.45%C) and on the other hand there is no sharp upper yield point for an Al alloy 2017-T4. This critical difference is considered to be based upon the constitutive equations themselves, Eqs. (1) and (3), as theoretically expected by calculations in Section 2. It should be noted that the breaking strains are also satisfactorily recorded. Machine A gives precise recordings of high-velocity tensile stress-strain relations for BCC and FCC materials. Machine B also do satisfactorily in spite of its narrow tensile velocity range. Its simplicity is of the same degree as Charpy or Izod type impact tests, but the results obtained may be directly applied as design data.

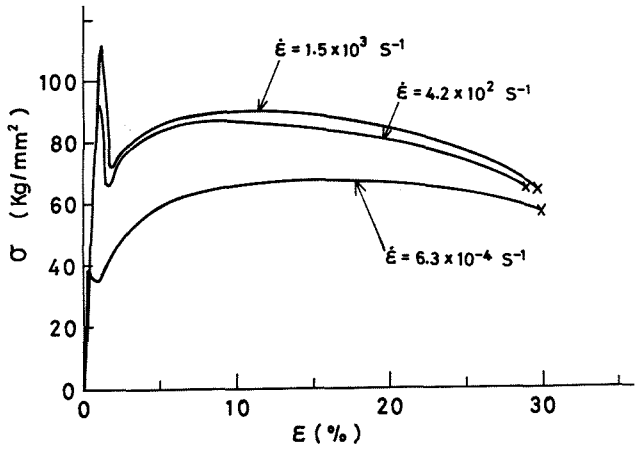

Figure 10. Typical experimental results obtained by machine A for a mild steel S45C.

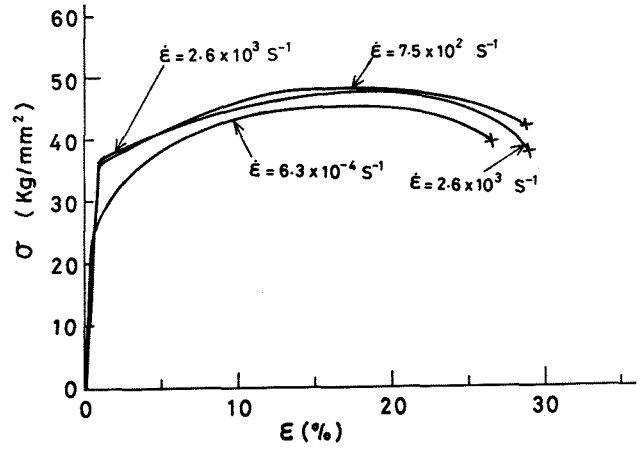

Figure 11. Typical experimental results obtained by machine A for 2017-T4 Al alloy.

4.2 Composite Materials

Composite materials are also powerful aerospace materials of high specific strength and specific stiffness. The above-mentioned one bar method is applied to the analysis of dynamic tensile behaviour of composite materials. By a series of high-velocity tension tests of typical fiber-reinforced plastics, very interesting and important dynamic tensile behaviours are revealed.

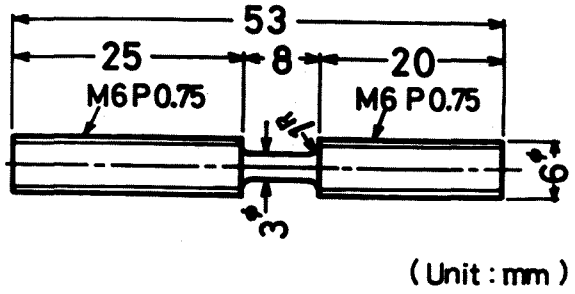

Figure 12. Dimensions of straight specimens.

4.2.1 Straight Specimens[15-17]. First, dynamic tensile tests using straight specimens shown in Fig. 12 are conducted. As shown in Table 2, tested materials cover ten different kinds of composite materials. They are divided into three groups, that is, glass/epoxy or polyester (denoted by G), carbon/epoxy (C) and injection-molded carbon or glass short fiber/nylon 66 (I). Three different kinds of woven cloth (plain, satin and semi-unidirectional satin) are tested for GFRP, although only plain woven cloths for CFRP. The ratio of the high strain rate nearly equal to 1×10^{3} /s to the low strain rate nearly equal to 1×10^{-3}/s, is nearly equal to 10^{6}, in this series of experiments. In Table 2, D and S denote dynamic and static cases, respectively. Definitions of tensile strength σ_p, and two strain values: ε_p and ε_t are shown in Fig. 13. E_{ab} is absorbed energy per unit volume in

Table 2. Tested materials and experimental results in dynamic and static tension.

No.	Composite system	D or S	No. of spec.	$\dot{\varepsilon}$ (sec^{-1})	σ_p (kg/mm^2)	ε_p (%)	ε_t (%)	E_{ab} (kg/mm^2)	Fiber, Resin, Manufacturer, Fiber volume fraction
G1	glass/polyester satin woven cloth	D	6	1.81×10^{3}	56.6	6.8	9.1	3.59	Asahi Fiber Glass SLS 212; Dainippon Ink&Chem., Polylite 8010; Asahi Fiber Glass Co., Ltd; V_f = 42.3%
		S	3	1.04×10^{-3}	33.1	4.16		0.784	
G2	glass/polyester satin woven cloth	D	7	2.03×10^{3}	50.9	8.3	9.8	3.05	Nittobo WE 181-BV; Dainippon Ink&Chem., Polylite 8010; Nitto Boseki Co., Ltd; V_f = 40.8 %
		S	4	1.18×10^{-3}	29.4	4.41		0.789	
G3	glass/epoxy satin woven cloth	D	5	2.12×10^{3}	53.5	6.9	7.8	2.51	Nittobo WE 181-BV; Shell Epicote 828; Nitto Boseki Co., Ltd; V_f = 39.4 %
		S	4	1.17×10^{-3}	32.5	4.77		0.904	
G4	glass/polyester plain woven cloth	D	5	1.79×10^{3}	46.8	7.9	10.1	3.41	Asahi Fiber Glass MS 252; Dainippon Ink&Chem., Polylite 8010; Asahi Fiber Glass Co., Ltd; V_f = 39.6 %
		S	3	1.05×10^{-3}	28.1	4.37		0.721	
G5	glass/epoxy plain woven cloth	D	5	1.90×10^{3}	58.8	7.5	8.6	2.69	Nippon Glass Fiber EMH 2503; Shell Epikote 828; Koei Industy; V_f = 43.3 %
		S	4	0.950×10^{-3}	34.4	3.56		0.720	
G6	glass/polyester semi-unidirectional satin woven cloth	D	3	0.582×10^{3}	78.8	9.7	14.3	8.04	Asahi Fiber Glass SCFE-182; Dainippon Ink&Chem., Polylite 8010; Asahi Fiber Glass Co., Ltd; V_f = 41.9 %
		S	3	0.874×10^{-3}	47.6	3.49		0.980	

No.	Composite system	D or S	No. of spec.	$\dot{\varepsilon}$ (sec^{-1})	σ_p (kg/mm^2)	ε_p (%)	ε_t (%)	E_{ab} (kg/mm^2)	Fiber, Resin, Manufacturer, Fiber volume fraction
C1	carbon/epoxy plain woven cloth	D	6	1.86×10^{3}	67.1	2.22	3.26	1.12	Torayca cloth #6343; Toray epoxy #2500; Toray Industries, Inc.; V_f = 53 %
		S	3	0.986×10^{-3}	56.5	3.30		0.995	
C2	carbon/epoxy plain woven cloth	D	4	2.07×10^{3}	50.2	2.84	5.05	1.22	Nippon Carbon, Carboron Z2pp; Shell Epikote 828; Koei Industry; V_f = 55 %
		S	2	1.13×10^{-3}	53.6	4.63		1.42	

No.	Composite system	D or S	No. of spec.	$\dot{\varepsilon}$ (sec^{-1})	σ_p (kg/mm^2)	ε_p (%)	ε_t (%)	E_{ab} (kg/mm^2)	Fiber, Resin, Manufacturer, Fiber volume fraction
I1	carbon/nylon 66 injection molding (short fiber)	D	6	0.704×10^{3}	11.3	1.68	2.00	0.130	Torayca chopped fiber; Toray nylon 66; Toray Industries, Inc.; V_f = 30 %
		S	3	0.997×10^{-3}	9.3	2.86		0.163	
I2	Glass/nylon 66 injection molding (short fiber)	D	7	0.670×10^{3}	9.9	1.70	2.14	0.132	Torayca chopped fiber; Toray nylon 66; Toray Industries, Inc; V_f = 30 %
		S	3	0.994×10^{-3}	13.9	4.05		0.341	

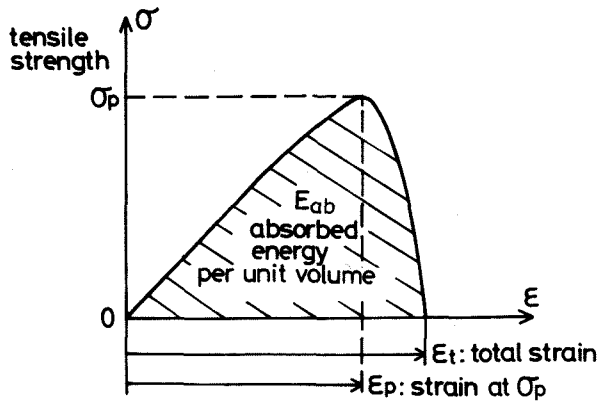

Figure 13. Defintions of two strain values.

fractured specmens. The details of tested materials and obtained results are shown in Table 2. Typical dynamic stress-strain diagrams in comparison with the corresponding static ones for some GFRP and CFRP specimens are shown in Fig. 14. Figure 15 shows strain rate dependence of σ_p, ε_p, ε_t and E_{ab}. Absolute value comparison of dynamic and static values are shown in Table 3.

These results are summarized as follows: For GFRP, all σ_p, ε_p, ε_t and E_{ab} increase with increasing strain rate, for all types of cloths and both matrices of epoxy and polyester. These strain rate dependences are defined as strain rate strengthening, ductilizing and toughening, respectively. From these results GFRP is considered to have suitable shock absorbing ability in high strain rate. On the contrary, CFRP seems to be different in high-velocity tensile behaviour. For CFRP, the variation of tensile strength and breaking strain with increasing strain rate is not so remarkable and the strain rate dependence is slightly positive or negative. When CFRP is used for the structure subjected to impact loading, this characteristic should be kept in design considerations. To utilize the superiority of CFRP in specific strength and specific stiffness in static loading and the merit of GFRP in dynamic loading, hybrids of these two materials or some other combinations of the same object would be effective.

From the sketches of fracture appearances of GFRP and CFRP shown in Fig. 16, fracture appearances in static and dynamic tension of GFRP are clearly different. In dynamic tension, resin between fibers is broken into pieces and blown away, and only fiber bundles are left and show brush-like appearance. For CFRP, the fracture appearance in dynamic tension is similar with the static one and shows simple and rather flat fracture surfaces. These appearances seem to explain the difference in strain rate dependence of the absorbed energy. The origin of remarkable increasing of absorbed energy in dynamic tension of GFRP is supposed possibly based upon the incresing of the tensile fracture strain of glass fibers and at the same time upon suitable pull-outs.

For injection-molded nylon 66 reinforced by short fibers of glass or carbon, little strain rate dependence of mechanical properties can be seen in the present data.

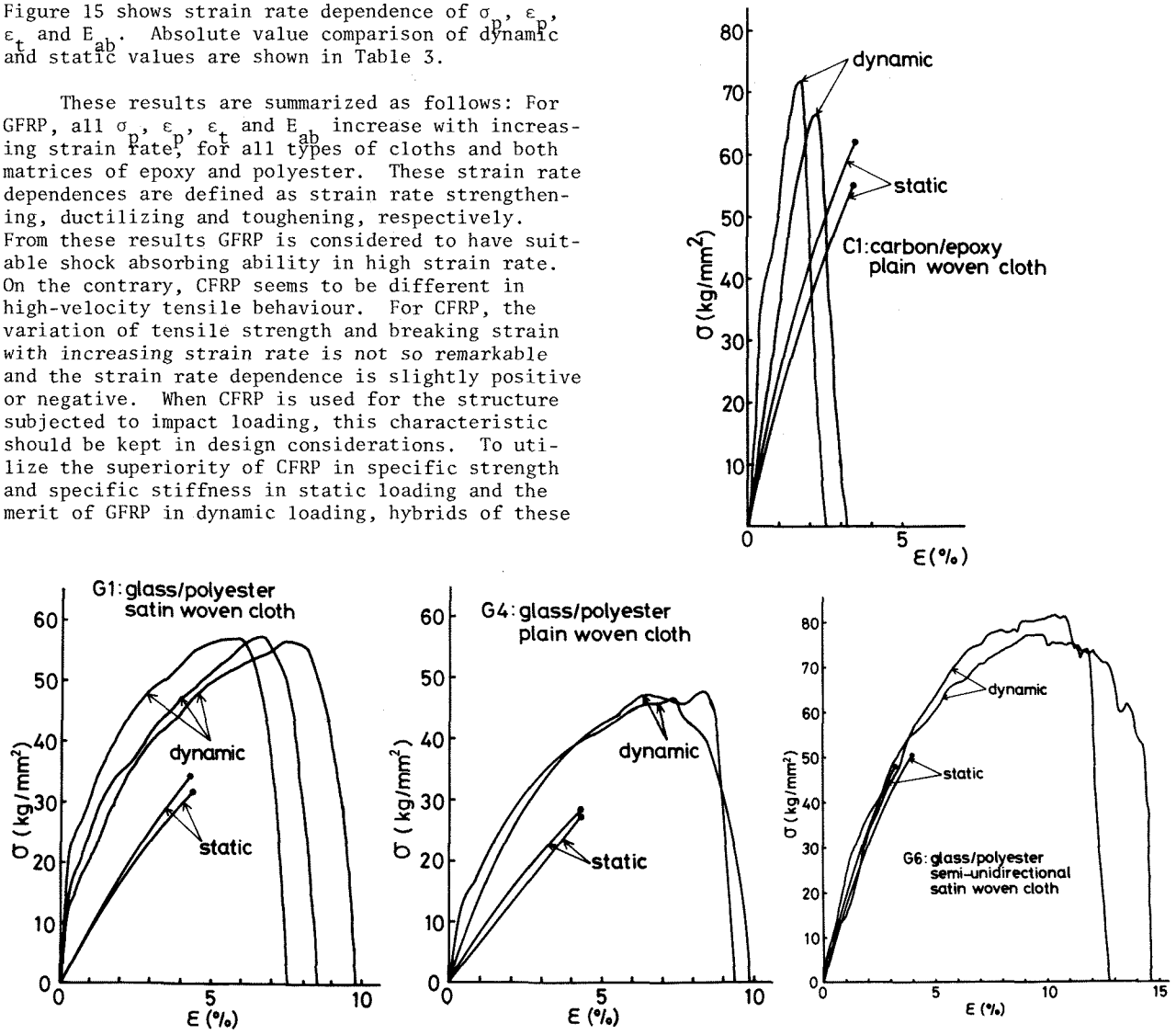

Figure 14. Typical dynamic and static stress-strain diagrams for some GFRP and CFRP specimens.

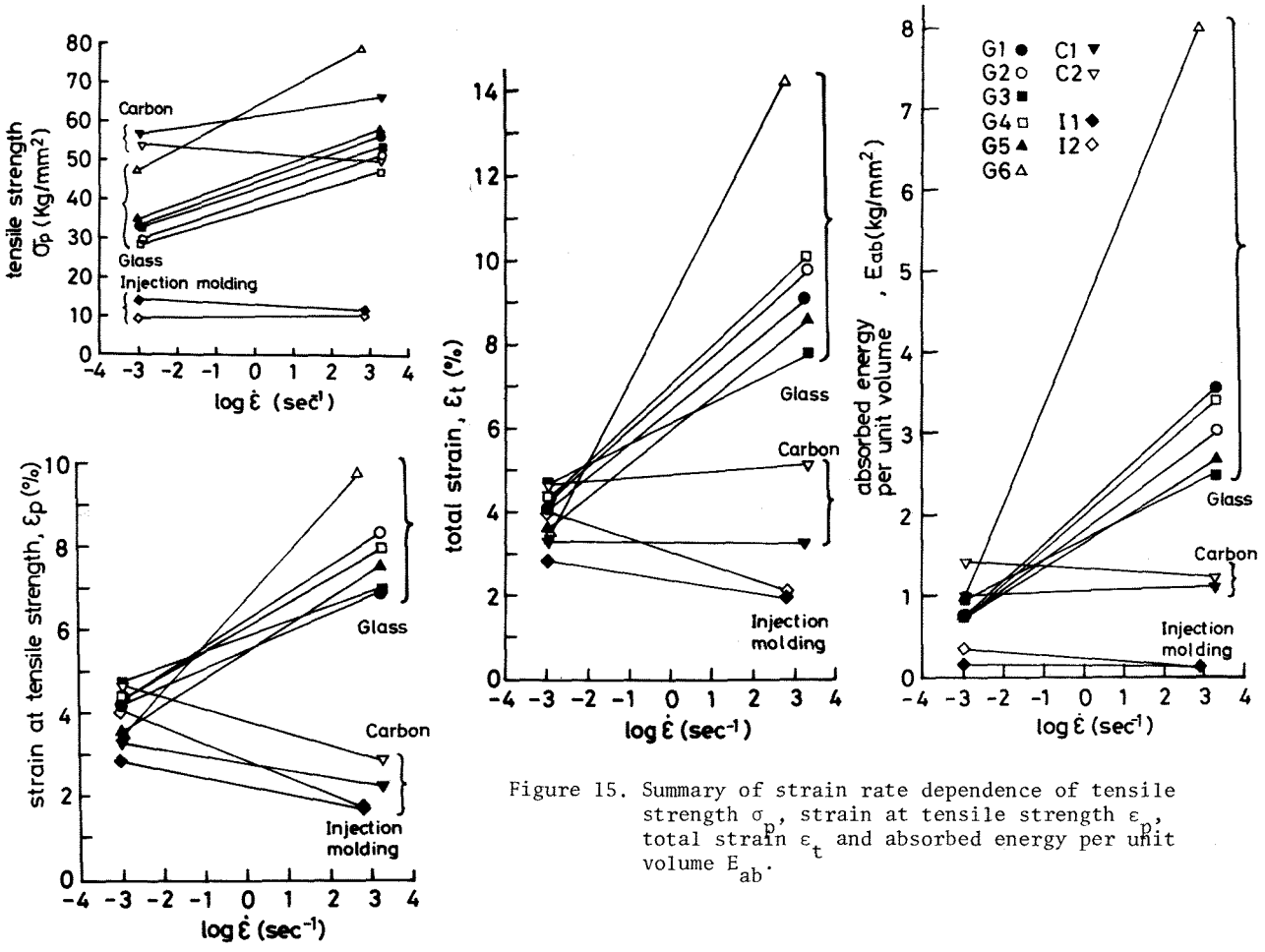

Figure 15. Summary of strain rate dependence of tensile strength σ_p, strain at tensile strength ε_p, total strain ε_t and absorbed energy per unit volume E_{ab}.

Table 3. Comparison of mechanical properties in dynamic tension with static values.

No.	$\frac{\sigma_{pd}}{\sigma_{ps}}$	$\frac{\varepsilon_{pd}}{\varepsilon_{ps}}$	$\frac{\varepsilon_{td}}{\varepsilon_{ts}}$	$\frac{E_{abd}}{E_{abs}}$
G1	1.71	1.63	2.19	4.58
G2	1.73	1.88	2.22	3.87
G3	1.65	1.45	1.64	2.78
G4	1.67	1.81	2.31	4.73
G5	1.71	2.11	2.42	3.74
G6	1.66	2.78	4.10	8.20
C1	1.19	0.67	0.99	1.13
C2	0.94	0.61	1.09	0.86

d: $\dot{\varepsilon} \cong 10^3$, s: $\dot{\varepsilon} \cong 10^{-3}$

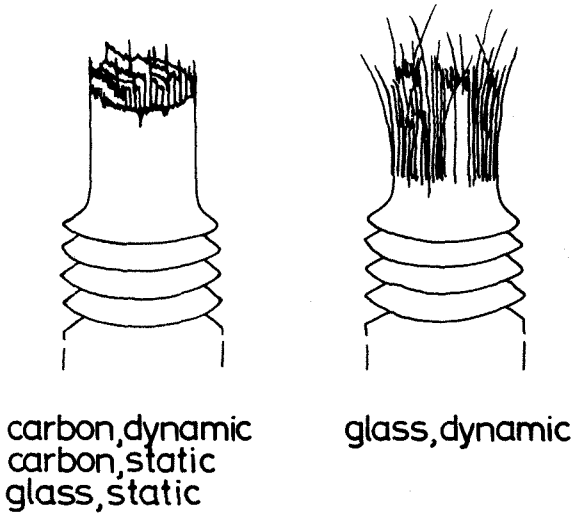

Figure 16. Fracture appearances of GFRP and CFRP in static and dynamic tension.

4.2.2 Circumferentially V Notced Specimens (Fig. 17) [17]. Using this type of specimen, fracture mechanical considerations may be made. In Table 4, σ_p is tensile fracture strength and 2γ is the total absorbed energy divided by the minimum cross-sectional area. The strain rate dependence of σ_p and 2γ are shown in Fig. 18. Although these values of γ are apparent ones, they would be useful for the measure of material properties in another standpoint. The γ values of glass/polyester in dynamic tension are considerably larger than those corresponding values of glass/epoxy. This fact is remarkable especially in plain-woven cloth. Generally the strain rate dependence of σ_p and 2γ of GFRP shown in Table 4 is positive. The effect of types of matrix resin and fiber surface treatment is large in γ value and not so clear in σ_p value. These facts mainly result from the difference in the fracture appearances. Debonding

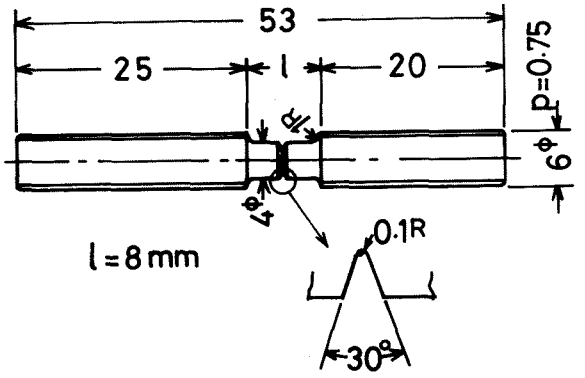

Figure 17. Circumferentially V notched specimens.

Table 4. Experimental results in dynamic and static tension of circumferentially V notched specimens.

Composite system	V_f (%)	cloth direc.	D or S	2γ kg·mm/mm²	σ_p kg/mm²	γ_d/γ_s	σ_{pd}/σ_{ps}
glass/polyester satin woven cloth SLS213-C-A	42.3	L	D	22.8	48.9	6.13	1.62
			S	3.72	30.1		
		T	D	24.8	46.6	5.71	1.45
			S	4.35	32.1		
" SLS213-C-B	47.3	L	D	23.3	48.3	6.46	1.64
			S	3.60	29.4		
		T	D	24.6	49.6	5.57	1.56
			S	4.42	31.7		
glass/epoxy satin woven cloth SLS213-E-A	40.3	L	D	16.3	47.1	4.30	1.50
			S	3.78	31.4		
		T	D	16.2	46.7	4.06	1.45
			S	3.99	32.1		
" SLS213-E-B	51.6	L	D	21.9	60.2	4.33	1.50
			S	5.05	40.3		
		T	D	18.9	56.4	3.77	1.41
			S	5.02	39.9		
glass/polyester plain woven cloth MS253-C-A	40.3	L	D	25.6	47.1	6.33	1.73
			S	4.05	27.3		
" MS253-C-B	48.4	L	D	44.2	53.2	8.94	1.54
			S	4.94	34.6		
glass/epoxy plain woven cloth MS253-E-A	38.1	L	D	20.3	44.6	7.40	1.73
			S	2.74	25.8		
" MS253-E-B	46.8	L	D	20.9	51.9	5.91	1.66
			S	3.53	31.3		
glass/polyester plain woven cloth MS252-A	40.5	L	D	31.7	43.2	7.89	1.61
			S	4.02	26.8		
glass/epoxy semi-unidirectional SCF-E-182	42.2	L	D	46.1	79.8	8.40	1.58
			S	5.48	50.5		

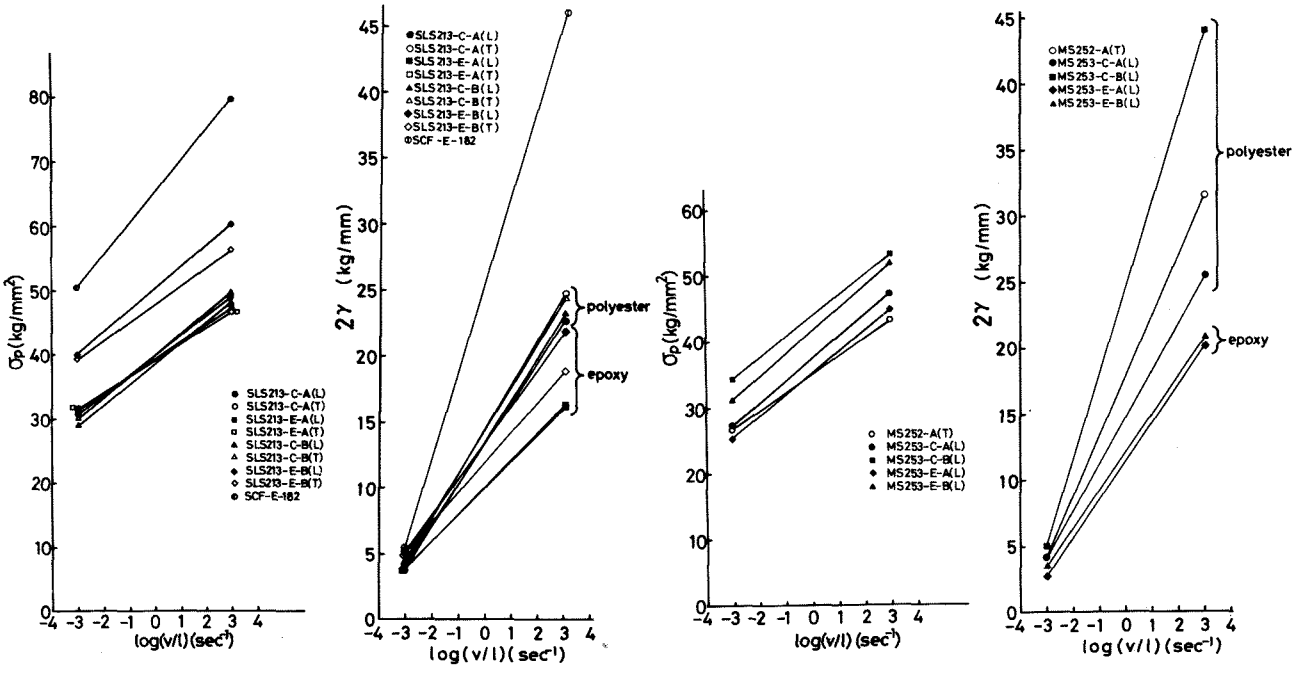

satin-woven cloth and semi-unidirectional cloth

plain-woven cloth

Figure 18. Strain rate dependence of tensile strength σ_p and fracture surface energy 2γ of circumferentially V notched specimens. (v: a terminal impact velocity).

between fibers and matrix and the following fiber pull-outs become more apparent in the order of glass satin- (or plain-) woven cloth/epoxy, glass satin-woven cloth/polyester and glass plain-woven cloth/polyester. So, this type of specimen may be useful to detect the effect of matrix type or surface treatment, which cannot be detected with straight specimens.

5. Summary and Conclusions

Systematic investigations of impact responses of various possible high-velocity tension testing systems have been conducted with specimens modelling BCC and FCC metals with their own constitutive equations of the microscopic origin. Through these investigations, one bar method of block-to-bar type has been found as a precise and simple system. Then a new testing machine of one bar method has been constructed and formulae for dynamic stress and strain have been derived. The major feature of this machine is that dynamic stress-strain diagrams can be obtained up to the breaking strain immediately after the test. With this new testing machine, typical aerospace materials have been tested, including metals (BCC and FCC) and composite materials (GFRP and CFRP), and new concepts of high-velocity ductility and brittleness have been introduced for both metallic and composite materials.

A wide material characterization program in high-velocity tension using this system is in progress. Major efforts are concentrated for metallic materials on high-strength Al alloys, Ti alloys, superalloys and stainless steels which are used in aerospace, high-speed transportation, nuclear-reactor areas and so forth. To utilize merits of CFRP and GFRP in a wide strain-rate range, hybrids of CFRP and GFRP or of some other combinations would be effective. For composite materials, efforts will be concentrated on hybrids and composites with other types of fibers (such as Aramid fibers). The developed high-velocity tension testing machine can be revised to have the capability of low-temperature testing. The preliminary results have been obtained for GFRP[18] and more data will be accumulated in near future.

Appendix

Derivation of Formulae for Dynamic Tensile Stress and Strain, Eq. (4), of One Bar Method.

The governing equation for the one-dimensional and longitudinal elastic wave propagation in a bar is given by,

$$\frac{\partial^2 u}{\partial t^2} = c^2 \frac{\partial^2 u}{\partial x^2} \qquad \left(c=\sqrt{\frac{E}{\rho}}\right) \tag{A1}$$

where u is the longitudinal displacement at a distance x at a time t. E, ρ and c denote Young's modulus, the density and the longitudinal elastic wave propagation speed of the material. Let us consider only a wave propagating in the negative direction of x, then a solution of Eq. (A1) is given by

$$u = f(x+ct) \tag{A2}$$

using an arbitrary function f. By differentiation, we obtain

$$\frac{\partial u}{\partial x} = f'(x+ct), \qquad \frac{\partial u}{\partial t} = cf'(x+ct) \tag{A3}$$

and then

$$\frac{\partial u}{\partial t} = c\frac{\partial u}{\partial x} = c\varepsilon \tag{A4}$$

Now the above relations are applied to the one bar method shown in Fig. 6. The displacement at a point B is given by

$$u_B(t) = \int_0^t \frac{\partial u_B}{\partial t} dt = c\int_0^t \varepsilon_B dt \tag{A5}$$

The strain ε_B at a point B is related to the strain ε_g $(=\varepsilon_C)$ at a point C obtained from strain gages by

$$\varepsilon_B(t) = \varepsilon_g\left(t+\frac{a}{c}\right) \tag{A6}$$

where a is the distance between points B and C. From Eqs. (A5) and (A6), we obtain

$$u_B(t) = c\int_0^t \varepsilon_g\left(\tau+\frac{a}{c}\right)d\tau \tag{A7}$$

On the other hand, the displacement at a point A is given using an impact-block velocity V(t) by,

$$u_A(t) = \int_0^t V(\tau)d\tau \tag{A8}$$

Since the length of the specimen l is short compared with the wavelength of an incident wave, dynamic strain and stress in the specimen can be assumed to be uniform through the specimen length. (This assumption was validated by a FEM numerical analysis[19] of the present testing machine). Then the strain and the strain rate in the specimen is defined by,

$$\varepsilon(t) = \frac{u_A(t)-u_B(t)}{l} = \frac{1}{l}\int_0^t \left[V(\tau)-c\varepsilon_g\left(\tau+\frac{a}{c}\right)\right]d\tau \tag{A9}$$

$$\dot{\varepsilon}(t) = \left[V(t)-c\varepsilon_g\left(t+\frac{a}{c}\right)\right]/l \tag{A10}$$

For the stress in the specimen, considering the equilibrium of forces at a section B, we define $\sigma(t)$ by,

$$\sigma(t) = (S_0/S)E_0\varepsilon_B(t) = (S_0/S)E_0\varepsilon_g\left(t+\frac{a}{c}\right) \tag{A11}$$

where E_0 and S_0 are Young's modulus and the cross-sectional area of the output bar, and S is the cross-sectional area of the specimen. Eqs. (A9) and (A11) give the desired dynamic strain and stress.

Acknowledgments

The authors wish to express their hearty thanks to Professor J. Shioiri, University of Tokyo for his useful discussions, and to the former members of Kawata laboratory, Dr. S. Kuriyama, Dr. K. Kurokawa, Mr. A. Hondo and Mr. N. Kanayama for their kind and energetic assistance in carrying out a series of our works.

References

[1] K. Kawata, S. Fukui, J. Seino and N. Takada, "Some Analytical and Experimental Invetsigations on High Velocity Elongation of Sheet Metals by Tensile Shock," Behaviour of Dense Media Under High Dynamic Pressure (Proc. of Symp. HDP, IUTAM, Paris, 1967), Dunod, Paris, 1968, pp. 313-323.

[2] K. Kawata, S. Hashimoto and K. Kurokawa, "Analysis of High Velocity Tension of Bars of Finite Length of BCC and FCC Metals with Their Own Constitutive Equations," High Velocity Deformation of Solids (Proc. of IUTAM Symp., Tokyo, 1977), Springer-Verlag, Berlin, 1979, pp. 1-15.

[3] K. Kawata, "Micromechanical Study of High Velocity Deformation of Solids," Theoretical and Applied Mechanics (Proc. of 15th Int. Congr. of Theor. and Appl. Mech., Toronto, 1980), North-Holland, 1980, pp. 307-317.

[4] W. G. Johnston and J. J. Gilman, "Dislocation Velocities, Dislocation Densities, and Plastic Flow in Lithium Fluoride Crystal," J. Appl. Phys., Vol. 30, No. 2, 1959, pp. 129-147.

[5] W. G. Johnston, "Yield Points and Delay Times in Single Crystals," J. Appl. Phys., Vol. 33, No. 9, 1962, pp. 2716-2730.

[6] S. Kuriyama and K. Kawata, "Propagation of Stress Wave with Plastic Deformation in Metal Obeying the Constitutive Equation of the Johnston-Gilman type," J. Appl. Phys., Vol. 44, No. 8, 1973, pp. 3445-3454.

[7] D. L. Holt, S. G. Babcock, S. J. Green and C. J. Maiden, "The Strain Rate Dependence of the Flow Stress in Some Aluminum Alloys," Trans. Am. Soc. Metals, Vol. 60, No. 2, 1967, pp. 152-159.

[8] A. Seeger, "The Generation of Lattice Defects by Moving Dislocations, and Its Application to the Temperature Dependence of the Flow Stress of FCC Crystals," Phil. Mag., Vol. 46, No. 382, 1955, pp. 1194-1217.

[9] U. S. Lindholm and L. M. Yeakley, "Dynamic Deformation of Single and Polycrystalline Aluminum," J. Mech. Phys. Solids, Vol. 13, No. 1, 1965, pp. 41-53.

[10] U. S. Lindholm, "Some Experiments in Dynamic Plasticity Under Combined Stress," Mechanical Behaviour of Materials Under Dynamic Loads, U. S. Lindholm, ed., Splinger, Berlin, 1968, pp. 77-95.

[11] J. Shioiri, "Microscopic Side of Behaviors of Metallic Materials in High Strain Rate," Proc. 2nd Shock Technology Symp. (Univ. of Tokyo), 1975, pp. 115-122(in Japanese).

[12] N. M. Newmark, "A Method of Computation for Structural Dynamics," Proc. Am. Soc. Civil Engr., Vol. 85, No. EM3, 1959, pp. 67-94.

[13] S. Nakagiri and H. Shimooka, "A Note on the Finite Element Approach to the Plastic Wave Propagation in Metal Obeying the Strain Rate-Dependent Constitutive Equation," CAS Research Paper, Vol. 19, 1976, pp. 39-44.

[14] K. Kawata, S. Hashomoto, K. Kurokawa and N. Kanayama, "A New Testing Method for the Characterization of Materials in High Velocity Tension," Mechanical Properties at High Rates of Strain 1979 (Conf. Ser. No. 47), J. Harding, ed., Inst. of Phys., Bristol and London, 1979, pp. 71-80.

[15] K. Kawata, A. Hondo, S. Hashimoto, N. Takeda and H. L. Chung, "Dynamic Behaviour Analysis of Composite Materials," Composite Materials: Mechanics, Mechanical Properties and Fabrication (Proc. Japan-US Conf. on Comp. Mater., Tokyo, 1981), Japan Soc. for Comp. Mater., Tokyo, 1981, pp. 2-11.

[16] K. Kawata, S. Hashimoto, H. Hondo and N. Takeda, "Analysis of Dynamic Tensile Behaviour of Composite Materials (2)" Proc. of 7th Comp. Mater. Symp., Japan Soc. for Comp. Mater., 1981, pp. 28-31.

[17] K. Kawata, S. Hashimoto and N. Takeda, "Mechanical Behaviours in High-Velocity Tension of Composites," Proc. of Int. Conf. on Comp. Mater. IV (ICCM-IV) (Tokyo, 1982) (in preparation).

[18] K. Kawata, S. Hashimoto and N. Takeda, "On Mechanical Properties in High Velocity Tension of FRP at Low Temperature," Proc. of Int. Cryogenic Mater. Conf. (Kobe, 1982) (in press).

[19] K. Kanayama, Fundamental Study of a New Measuring Method of Tensile Impact Resistant Properties of Materials, M. E. thesis, Univ. of Tokyo, 1979.